BBA - Molecular Cell Research 1867 (2020) 118787

Contents lists available at ScienceDirect

BBA - Molecular Cell Research

journal homepage: www.elsevier.com/locate/bbamcr

Kinetic and protective role of autophagy in manganese-exposed BV-2 cells

Soledad Porte Alcon, Roxana Mayra Gorojod, Mónica Lidia Kotler*

CONICET- Universidad de Buenos Aires. Instituto de Química Biológica Ciencias Exactas y Naturales (IQUIBICEN). Facultad de Ciencias Exactas y Naturales, Departamento de Química Biológica, Laboratorio de Disfunción Celular en Enfermedades Neurodegenerativas y Nanomedicina. Ciudad Autónoma de Buenos Aires, Argentina

ARTICLE INFO

Keywords:
Microglia
Manganese
Autophagy
Lysosomes
Reactive oxygen species

ABSTRACT

Manganese (Mn) plays an important role in many physiological processes. Nevertheless, Mn accumulation in the brain can cause a parkinsonian-like syndrome known as manganism. Unfortunately, the therapeutic options for this disease are scarce and of limited efficacy. For this reason, a great effort is being made to understand the cellular and molecular mechanisms involved in Mn toxicity in neuronal and glial cells. Even though evidence indicates that Mn activates autophagy in microglia, the consequences of this activation in cell death remain unknown. In this study, we demonstrated a key role of reactive oxygen species in Mn-induced damage in microglial cells. These species generated by Mn^{2+} induce lysosomal alterations, LMP, cathepsins release and cell death. Besides, we described for the first time the kinetic of Mn^{2+}-induced autophagy in BV-2 microglial cells and its relevance to cell fate. We found that Mn promotes a time-dependent increase in LC3-II and p62 expression levels, suggesting autophagy activation. Possibly, cells trigger autophagy to neutralize the risks associated with lysosomal rupture. In addition, pre-treatment with both Rapamycin and Melatonin enhanced autophagy and retarded Mn^{2+} cytotoxicity. In summary, our results demonstrated that, despite the damage inflicted on a subset of lysosomes, the autophagic pathway plays a protective role in Mn-induced microglial cell death. We propose that 2 h Mn^{2+} exposure will not induce disturbances in the autophagic flux. However, as time passes, the accumulated damage inside the cell could trigger a dysfunction of this mechanism. These findings may represent a valuable contribution to future research concerning manganism therapies.

1. Introduction

Manganese (Mn) is a trace metal essential for human health. It is a cofactor of a variety of enzymes such as oxidoreductases, hydrolases, transferases, lyases, arginase, glutamine synthetase and superoxide dismutase [1]. Therefore, Mn is required for several physiological processes including immune response, brain functioning and development, regulation of blood sugar and cellular energy, and homeostasis and defense against reactive oxygen species (ROS) [2,3]. Diet is considered the primary source of Mn intake. Particularly, vegetarian diets are enriched in Mn compared with those of the omnivorous [4]. The recommended dietary allowances vary according to gender, age and health states [5]. However, like other micronutrients, this metal is required only in small quantities and higher concentrations may result in toxicity [6].

Excessive exposure to Mn can cause its accumulation in the central nervous system (CNS), predominantly in the basal ganglia, leading to an extrapyramidal syndrome known as manganism [7–9]. Patients with this condition have symptoms that resemble Parkinson's Disease, such as bradykinesia, rigidity and muscle tremors, gait disturbance, postural instability and dystonia and/or ataxia. Additionally, psychiatric disorders and cognitive deficits have also been reported [7]. Mn neurotoxicity was first described by Couper [10] in workers grinding the black oxide of Mn, pyrolusite (MnO_2). Since then, manganism has been diagnosed in various occupational settings in which workers are exposed to Mn-laden dust like mining, welding, smelting, and in steel, aluminum and dry battery manufacturing [11]. These industrial activities also affect general population by increasing Mn concentration in the environment. Additional anthropogenic sources include the employment of fungicides (maneb and mancozeb), water purification agents (permanganate), and the fuel additive MMT (methylcyclopentadienyl manganese tricarbonyl). Environmental Mn exposure is also a potential health risk, since it has been related to a higher prevalence of Parkinsonian disorders and other neurological disturbances [12,13].

Microglia are the resident innate immune cells in the brain and constitute the first line of defense against pathogens, foreign material, and dead or dying cells. In the presence of any of these stimuli,

* Corresponding author.
E-mail addresses: sportealcon@qb.fcen.uba.ar (S. Porte Alcon), rgorojod@qb.fcen.uba.ar (R.M. Gorojod), kotler@qb.fcen.uba.ar (M.L. Kotler).

https://doi.org/10.1016/j.bbamcr.2020.118787
Received 27 February 2020; Received in revised form 1 June 2020; Accepted 22 June 2020
Available online 24 June 2020
0167-4889/

microglia become activated to restore brain homeostasis [14,15]. However, sustained microglial activation and neuroinflammation have been associated with neuronal loss in neurodegenerative diseases, including Parkinson's Disease (PD), Alzheimer's Disease and Huntington Disease [16]. Similarly, the contribution of microglia to neurodegeneration in manganism has been documented ([17] and cited references). Nevertheless, the mechanisms leading to Mn toxicity in microglia have been poorly explored. Oxidative stress is a key player in Mn toxicity. Mn-induced activation of both astrocytes and microglia promotes the release of ROS and reactive nitrogen species (RNS), which contribute to oxidative stress conditions [17,18]. Reactive species oxidize biomolecules, such as proteins, lipids and DNA, leading to cell damage and, ultimately, cell death. However, in certain contexts cells can recover from this type of injury [19].

Macroautophagy (hereafter referred to as “autophagy”) is a catabolic pathway in which cytoplasmic components, such as long-lived proteins and dysfunctional organelles, are sequestered and transported to lysosomes for degradation. Autophagy is a well-coordinated process that involves multiple steps. First, cargo is sequestered into a transient membrane known as phagophore. This compartment expands until the cargo is engulfed and form a double-membrane vesicle termed autophagosome. This step requires the lipidation of Microtubule-Associated Protein 1 Light Chain 3 (LC3-I). Briefly, the cytosolic LC3-I becomes conjugated to phosphatidylethanolamine via a series of ubiquitin-like reactions. This lipid- modified form of LC3 (LC3-II) is then recruited and incorporated into the autophagosomal membrane. Finally, the autophagosome fuses with the lysosome. In this vesicle termed autolysosome, the cargo is degraded by acidic hydrolases and the resulting macromolecules are recycled [20]. SQSTM1/p62 is also a relevant protein for the autophagic process. It is a multifunctional protein that interacts with LC3 and transports ubiquitinated proteins and organelles for degradation by the autophagosome. It becomes incorporated into the completed autophagosome and is degraded in autolysosomes [21].

Autophagy is induced by a variety of stress stimuli including oxidative stress [22,23]. The simultaneous activation of autophagy and the antioxidant response is aimed at restoring cell homeostasis by decreasing ROS/RNS concentration and reducing oxidative damage [24]. However, autophagy also plays a role in programmed cell death, neurodegeneration and aging [25]. Although few studies have focused on Mn-induced autophagy [26], its protective role in both neurons [27–31] and astrocytes [32] has been reported. Regarding microglia, Wang et al. [33] and Chen et al. [34] have demonstrated that Mn promotes autophagic dysfunction. However, the role of autophagy in Mn-induced microglial cell death has not been addressed yet.

We have previously described the complex molecular signaling pathways involved in Mn-induced BV-2 microglial cell death. We demonstrated that Mn triggers cell death by regulated necrosis, involving both *parthanatos* and lysosomal disruption. In this model ROS production was partially responsible for Mn-induced cytotoxicity [35]. In the current study, we deepen our knowledge about the implication of ROS in both lysosomal damage and cytotoxicity. Besides, our results describe for the first time the kinetic of the Mn-induced autophagy in BV-2 cells and their impact on cell survival. We propose that autophagy is triggered as a rescue mechanism in an attempt to protect cells from lethal effects of Mn.

2. Materials and methods

2.1. Reagents

Roswell Park Memorial Institute medium (RPMI-1640), manganese chloride, trypsin, Hoechst 33258 fluorochrome, phenylmethylsulfonyl fluoride (PMSF), bis-benzamidine, ECL detection reagents (luminol and p-coumaric acid), Polyethylenimine (PEI) branched MW 25,000 and Melatonin (Mel) were purchased from Sigma Chemical Co. (St. Louis, MO, USA). Fetal bovine serum (FBS) was obtained from Natocor (Córdoba, Argentina). Streptomycin, penicillin and amphotericin B were from Richet (Buenos Aires, Argentina). 3-(4,5-Dimethyl-thiazol-2-yl)-2,5-diphenyl-tetrazolium bromide (Thiazolyl Blue Tetrazolium Bromide, MTT) and aprotinin were purchased from Santa Cruz Biotechnology (Dallas, TX, USA). The acidic vacuole-specific red fluorescent probe LysoTracker Red DND-99 was from Molecular Probes (Eugene, OR, USA).

The following antibodies were employed: MAP LC3β (N-20) sc-16,755, anti-actin (C4) sc-47,778, anti- mouse IgG-HRP sc-2031 and anti-rabbit IgG-HRP sc-2030 were purchased from Santa Cruz Biotechnology; LC3B #2775 and SQTM1/p62 #5114 were from Cell Signaling Technology, Inc. (Danvers, MA, USA); anti-α-tubulin ab4074 was purchased from Abcam (Cambridge, UK); anti-goat IgG (H + L) Alexa Fluor 555 #A-21432 was purchased from Invitrogen (Thermo Fisher Scientific). The following inhibitors were assayed: Bafilomycin A1 (BafA1) from Fermentek (Jerusalem, Israel); Wortmannin (Wort) from Calbiochem (La Jolla, CA, USA); and Rapamycin (Rapa) from Sigma Aldrich Co. The final concentration of vehicle (DMSO) did not exceed 0.12% and not affect cell viability, morphology or other parameters tested in this study. All other chemicals used were of the highest purity commercially available.

2.2. Cell culture and manganese exposure

BV-2 murine microglial cells, immortalized by infection with v-raf/c-myc recombinant retrovirus [36], were kindly provided by Dr. Fernando Correa (CEFYBO-CONICET, Argentina). Cells were maintained in RPMI-1640 supplemented with 10% heat-inactivated FBS, 2.0 mM glutamine, 100 units/mL penicillin, 100 μg/mL streptomycin and 1.25 μg/mL amphotericin B. Cells were cultured at 37 °C in a humidified atmosphere of 5% CO_2-95% air, and the medium was renewed three times a week. For all experiments, BV-2 cells were removed with 0.25% trypsin-EDTA and diluted with RPMI-1640 10% FBS. According to the experiment, cells were re-plated into Petri dishes or multi-well plates at a density of 2.5–5 × 10^4 cells/cm^2. After 24 h in culture, cells reaching ~70–80% confluence were exposed to 250 or 750 μM $MnCl_2$ (Mn^{2+}) in RPMI-1640 supplemented with 2% FBS [35]. Cells were pretreated with Wort, Mel or Rapa for 1 h prior to Mn^{2+} treatment. BafA1 (100 nM) was added 2 h before the end of the experiments.

2.3. Plasmid and transfection

The GFP-mCherry-LC3B expression plasmid was kindly provided by Dr. Juan Bonifacino (Cell Biology and Neurobiology Branch, NICHD, NIH, Bethesda, MD, USA). Transfection was performed according to Pomilio et al. [37] with slight modifications. BV-2 cells were seeded on coverslips in 24-well plates and allowed to grow for 24 h until 50–60% confluence. Transfection complexes were prepared in serum-free media in a ratio PEI:DNA 3.5:1. Mixtures were vortexed, incubated 10 min at RT and drop-wise added to cells in serum media. After 4 h, media was renewed. All experiments were performed at 24 h post-transfection.

2.4. Neutral Red uptake assay

Neutral Red (NR) is a weakly cationic dye that penetrates cell membranes by non-ionic passive diffusion and concentrates in the lysosomes, where it binds to anionic and/or phosphate groups in the lysosomal matrix through electrostatic hydrophobic bond. As such, the NR uptake assay allows assessing the lysosomal integrity [38,39]. The experiments were carried out following the protocol described by Repetto et al. [38] with slight modifications. NR solution (40 μg/mL in RPMI-1640) was prepared and incubated overnight (ON) at 37 °C. Before its use, the solution was centrifuged at 2600 rpm for 10 min to remove undissolved crystals. After Mn^{2+} exposure, cells grown on 96-well plate were washed with PBS and incubated with 200 μL NR solution at 37 °C. After 2 h, dye retention was examined by phase-contrast

microscopy (Olympus IX71, Olympus Corporation, Tokyo, Japan). Images were taken with an ORCA-ER camera (Hamamatsu Photonics K.K., Systems Division, Hamamatsu, Japan) and assembled with Adobe Photoshop 7.0 software. Next, cells were washed once with PBS and 200 μL of acid alcohol solution (1% v/v acetic acid in 50% ethanol) was added to each well until complete dye dissolution. Absorbance was measured at 570 nm with background subtraction at 690 nm in a BIO-RAD Model 680 Benchmark microplate reader. Results were expressed as a percentage of control cells.

2.5. Detection and quantification of acidic vesicular organelles (AVOs)

AVOs were detected by LysoTracker Red DND-99 (λem: 577 nm, λem: 590 nm) staining as described by Gorojod et al. [29] with slight modifications. After treatments, cells were washed with PBS and stained with 500 nM LysoTracker in serum-free medium for 30 min at 37 °C. Next, AVOs were analyzed by flow cytometry or fluorescence microscopy as described below.

For FACS analysis, cells grown on 12-well plates were washed twice with PBS and harvested by detachment with 100 μL trypsin-EDTA. Subsequently, 1.5 mL PBS was added and cells were transferred to Eppendorf tubes. Briefly, cell suspensions were centrifuged at 1000 rpm for 5 min and the resultant pellets resuspended in 500 μL PBS. Samples were kept on ice and protected from light until measurement. Forward and side scatters were used to exclude debris and dead cells. Fluorescence emission of at least 10,000 events/sample was measured with a FACS Aria II flow cytometer (BD Biosciences, San Jose, CA, USA) (λex: 488 nm; λem: 585/42 nm; FL-2). Data was analyzed employing FlowJo 7.6 software (Tree Star, OR, USA).

For fluorescence microscopy analysis, cells grown on coverslips were washed with PBS, fixed with 4% paraformaldehyde/4% sucrose (PFA 4%) in PBS for 30 min at room temperature (RT) and washed five times with PBS. Next, coverslips were mounted on glass slides with PBS-glycerol (1:1, v/v) and examined under an Olympus IX71 fluorescence microscope (λex: 510–550 nm; λem: LP 590 nm) equipped with an ORCA-ER camera. Images obtained were analyzed with ImageJ software (U.S.National Institutes of Health, Bethesda, MD, USA). To measure the LysoTracker Red fluorescence intensity, the product between the mean fluorescence intensity (MFI) and the area of each cell was calculated (100 cells/sample). To determine AVOs diameter (D), a selected area surrounding each AVO was drawn and a manual threshold was applied to distinguish between adjacent vacuoles avoiding the quantification of non-specific fluorescent pixels. The area of individual AVOs from 25 cells was measured (500 AVOs/sample) and the D was calculated as:

$$D = 2\sqrt{\frac{area}{\pi}}$$

2.6. Immunocytochemistry

Immunocytochemistry was performed according to Gorojod et al. [32]. PFA 4%-fixed samples were washed five times with PBS, permeabilized with 0.25% Triton X-100 in PBS for 10 min at RT and washed three times with PBS. Then, cells were blocked in 1% bovine serum albumin (BSA)-PBST (137 mM NaCl; 2.68 mM KCl; 10 mM Na_2HPO4; 1.76 mM KH_2PO4; 0.05% Tween 20; pH 7.4) ON at 4 °C. Coverslips were incubated with anti-MAPLC3β primary antibody (1:100) for 1 h at RT, washed three times with PBS and incubated with an anti-goat IgG-Alexa555 secondary antibody (1:1000) for 1 h at RT. Nuclei were counterstained with 1.5 μg/mL Hoechst 33258 for 10 min at RT in the dark. Finally, coverslips were mounted and analyzed under an Olympus IX71 fluorescence microscope. Digital images were processed with ImageJ and assembled using Adobe Photoshop 7.0 software. To quantify LC3 expression, the product between the MFI and the area of each cell was calculated (100 cells/sample).

2.7. Western blots

Western blots were performed according to Alaimo et al. [40] with slight modifications. After treatment, floating cells were harvested and reserved on ice, while adherent cells were detached by scrapping. Cellular suspensions were pooled together, centrifuged at 1000 rpm for 5 min at RT and washed once on ice-cold PBS. Then, cells were lysed in lysis buffer (50 mM HEPES/0.1% Triton pH 7.0, 0.5 mM PMSF, 10 mg/mL aprotinin and 10 mg/mL benzamidine) for 30 min in an ice-bath and sonicated (40% amplitude, 15 s) in a Sonics VCX-750 Vibra Cell Ultra Sonic Processor (Sonics & Materials, Inc., Newtown, CT, USA). Cell lysates were centrifuged (12,000 ×*g*, 20 min, 4 °C) and protein concentration in supernatants was determined using Bradford assay. An equal amount of proteins (60–80 μg) from each treatment was separated on 10, 12 or 13.5% SDS- PAGE and blotted onto nitrocellulose membranes (Hybond ECL, GE Healthcare, Piscataway, NJ). Transference efficiency was verified by staining the membrane with Ponceau Red. Non-specific binding sites were blocked by 5% non-fat dried milk in TBS (150 mM NaCl in 50 mM Tris-HCl buffer pH 8) containing 0.1% SDS (90 min) and then incubated with specific antibodies ON at 4 °C. The primary antibody reaction was followed by incubation for 1 h with horseradish peroxidase-conjugated secondary antibodies. All antibodies were diluted in TBST (150 mM NaCl, 0.05% Tween 20, in 50 mM Tris-HCl buffer pH 8) with 3% non-fat milk. Immunoreactive bands were detected by chemiluminescence using ECL detection reagents and images were captured with an Amersham Imager 600 (GE Healthcare) imaging system. Quantitative changes in protein levels were evaluated employing ImageJ software. The molecular weight of proteins was estimated by electrophoresis of the PageRuler Prestained Protein Ladder (Thermo Scientific Inc., Waltham, USA). To confirm equal protein loading in each lane, antibodies were stripped from the membranes with stripping buffer (15% H_2O_2 in TBS) and re-probed with a loading control.

2.8. MTT reduction assay

The MTT assay was carried out to evaluate cell viability according to the protocol previously described [41] with slight modifications. BV-2 cells were incubated with MTT solution (final concentration of 62.5 μg/mL) for 2 h at 37 °C. The resulting formazan crystals were solubilized in DMSO (200 μL per well). Absorbance was measured at 570 nm with background subtraction at 655 nm in a DR-2000Bs microplate reader (Diatek Instruments Co. China). The MTT reduction activity was expressed as a percentage of the control cells.

2.9. Autophagic flux assay with GFP-mCherry-LC3B plasmid

The autophagic flux was measured in GFP-mCherry-LC3B-transfected BV-2 cells using an imaging-based assay [42]. This assay is based in the differential stability of GFP and mCherry at acidic pH: while mCherry fluorescence remains stable, that of GFP is quenched. Consequently, at the neutral pH of autophagosomes both the GFP (green) and mCherry (red) proteins fluoresce, whereas in the acidic pH of autolysosomes only the red fluorescence is visible. Thus, the relative amount of autophagosomes (yellow puncta) and autolysosomes (red puncta) in each cell can be determined [20]. After treatments, cells were washed with PBS, fixed with PFA 4% for 30 min at RT and washed five times with PBS. Next, coverslips were mounted on glass slides with PBS-glycerol (1:1, v/v) and examined under an Olympus FV1000 laser confocal scanning microscope (Olympus Corporation, Tokyo, Japan). Digital images were processed with ImageJ and assembled using Adobe Photoshop 7.0 software. To analyze autophagic flux, the number of yellow (autophagosomes) and red (autolysosomes) LC3 puncta per cell were quantified (20 cells/sample).

2.10. Statistical analysis

Experiments were carried out in triplicate unless otherwise stated. Results are expressed as mean ± standard error of the mean (SEM) values. Experimental comparisons between treatments were made by one- or two- way ANOVA, followed by Student- Newman-Keuls post hoc test with statistical significance set at $p < 0.05$. Student's *t*-test with Welch's correction indicated that inter-experiment variations in western blot signals are not significantly different ($p > 0.05$). All analysis was carried out with GraphPad Prism 5 software (San Diego, CA, USA).

3. Results

3.1. Mn^{2+} causes a ROS-mediated expansion of the lysosomal compartment in BV-2 cells

Previous results from our group have demonstrated that Mn^{2+} induces lysosomal membrane permeabilization (LMP) and cathepsin D (CatD) release into the cytosol in BV-2 cells supporting the occurrence of lysosomal disruption [35]. To deepen our knowledge about the effect of Mn^{2+} on lysosomal integrity we first performed a NR retention assay. Exposure to 250 and 750 μM Mn^{2+} decreased a 43.1 ± 1.5% ($p < 0.001$) and 51.6 ± 1.4% ($p < 0.001$) NR retention, respectively (Fig. 1a). However, phase-contrast microscopy analysis revealed higher dye retention in Mn^{2+}-treated cells in comparison with control cells (Fig. 1b). These results suggested that Mn^{2+} increases the number and/or size of lysosomes in microglial cells. Considering our previous reports demonstrating that i) ROS generation is implicated in Mn^{2+}-induced cell death in BV-2 cells [35] and ii) ROS negatively affect the integrity of the lysosomal membranes leading to the formation of enlarged AVOs in C6 cells [32], we next evaluated the possible involvement of ROS in NR retention by employing the antioxidant hormone Mel. Pre-treatment with 10 μM Mel prevented the reduction in NR retention a 10.2 ± 1.1% ($p < 0.001$) and 7.9 ± 1.2% ($p < 0.01$) at 250 and 750 μM Mn^{2+}, respectively (Fig. 1a), demonstrating that ROS play a role in metal toxicity. However, under these conditions no effect of Mel on NR retention could be confirmed by phase-contrast microscopy analysis (Fig. 1b).

In order to obtain additional evidence about lysosomal integrity, we performed a flow cytometry assay in BV-2 cells exposed to Mn^{2+} and stained with LysoTracker Red DND-99. As shown in Fig. 2a–b, Mn^{2+} increases LysoTracker Red fluorescence intensity. This observation may be explained by an increment in the size and/or number of lysosomes. To discern between both possibilities, we analyzed LysoTracker Red staining by fluorescence microscopy (Fig. 2c) and quantified the MFI per cell (Fig. 2d) and the diameter of lysosomes (Fig. 2e). While Mn^{2+} exposure induced an increase in the number of lysosomes, no alterations in the diameter of the vesicles were observed. Images of Fig. 2c are also consistent with alterations in both the distribution and the number of lysosomes.

The possible involvement of ROS in lysosomal events was investigated employing 10 μM Mel. Mel pre-incubation completely prevented the increase in the fluorescence intensity induced by Mn^{2+} ($p < 0.001$) without affecting the diameter of the vesicles (Fig. 2d and e). These results suggest that ROS could mediate the increment in the amount of lysosomes observed after Mn^{2+} exposure.

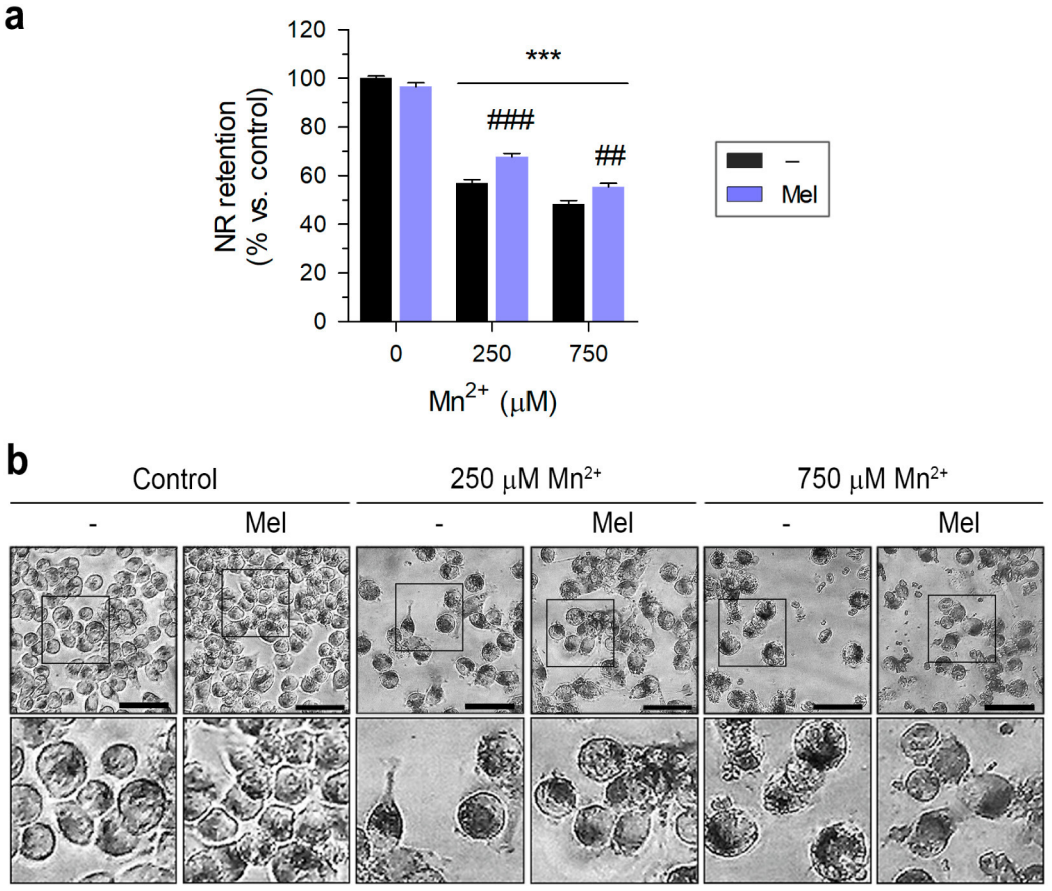

Fig. 1. Mn^{2+} expands the lysosomal compartment. BV-2 cells were pre-incubated (1 h) with Mel (10 μM) and exposed to Mn^{2+} (250 and 750 μM). After 24 h, NR retention assay was performed. (a) Values are expressed as a percentage of control cells. ***$p < 0.001$ vs control; ##$p < 0.01$ and ###$p < 0.001$ vs Mn^{2+}. (b) Phase-contrast microscopy analysis of NR retention. Representative images are shown. Lower panels denote magnification (2×) of the selected area. Scale bar: 50 μm.

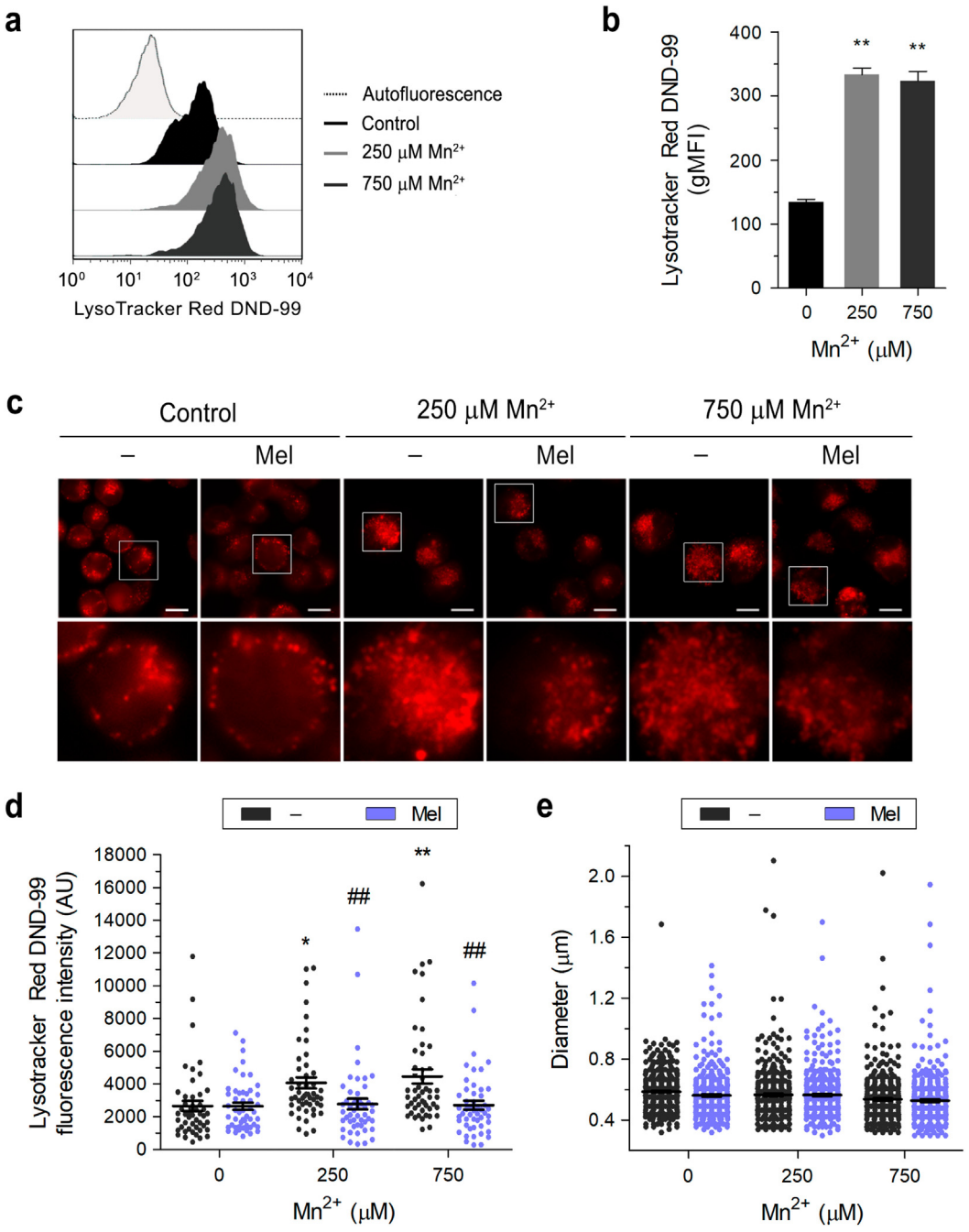

Fig. 2. Mn^{2+} alters both the number and distribution of AVOs. (a, b) BV-2 cells were exposed to Mn^{2+} (250 and 750 μM) for 24 h, stained with LysoTracker Red DND-99 (500 nM) and flow cytometry analysis was performed (λex: 488 nm; λem: 585/42 nm; FL-2) in 10,000 events/treatment. (a) Representative histograms are shown. (b) Quantification of the geometric mean fluorescence intensity (gMFI) of LysoTracker Red DND-99. (c–e) Cells were pre-treated (1 h) with Mel (10 μM) before Mn^{2+} exposure (250 and 750 μM, 24 h), and LysoTracker Red DND-99 staining was analyzed by fluorescence microscopy (λex: 510–550 nm, λem: LP 590 nm). Representative images are shown in (c). Lower panels denote magnification (4.6×) of the selected area. Scale bar: 10 μm. (d) Mean fluorescence intensity of LysoTracker Red DND-99 (50 cells/treatment) and (e) AVOs' diameter (400 AVOs/treatment) were measured employing ImageJ software. *$p < 0.05$ and **$p < 0.01$ vs control; ##$p < 0.01$ vs Mn^{2+}.

3.2. Mn^{2+} triggers the autophagic pathway in BV-2 cells

It is widely recognized that LMP may contribute to dysfunctional autophagy [43,44]. Thus, considering that damaged lysosomes are cleared by autophagy and autophagic degradation under oxidative stress conditions may result in lysosomal membranes damage [45], we next investigated the possible activation of the autophagic pathway.

It has been demonstrated that punctate LC3-labeled structures observed under microscopy represent autophagosomes [20]. Then, we first examined the effect of Mn^{2+} on the formation of LC3-labeled autophagosomes by immunocytochemistry (Fig. 3a).

Exposure to Mn^{2+} induced the formation of a typical LC3 puncta pattern in microglial cells. Quantitative analysis showed that 250 and 750 μM Mn^{2+} increase LC3 levels (MFI) at 250.8 ± 12.8% ($p < 0.001$) and 266.1 ± 3.9% ($p < 0.001$) respectively (Fig. 3b). These results suggest that the autophagic pathway is triggered by Mn^{2+}. The autophagosome formation can also be assessed by analyzing the increase in the levels of LC3-II by western blot. However, this

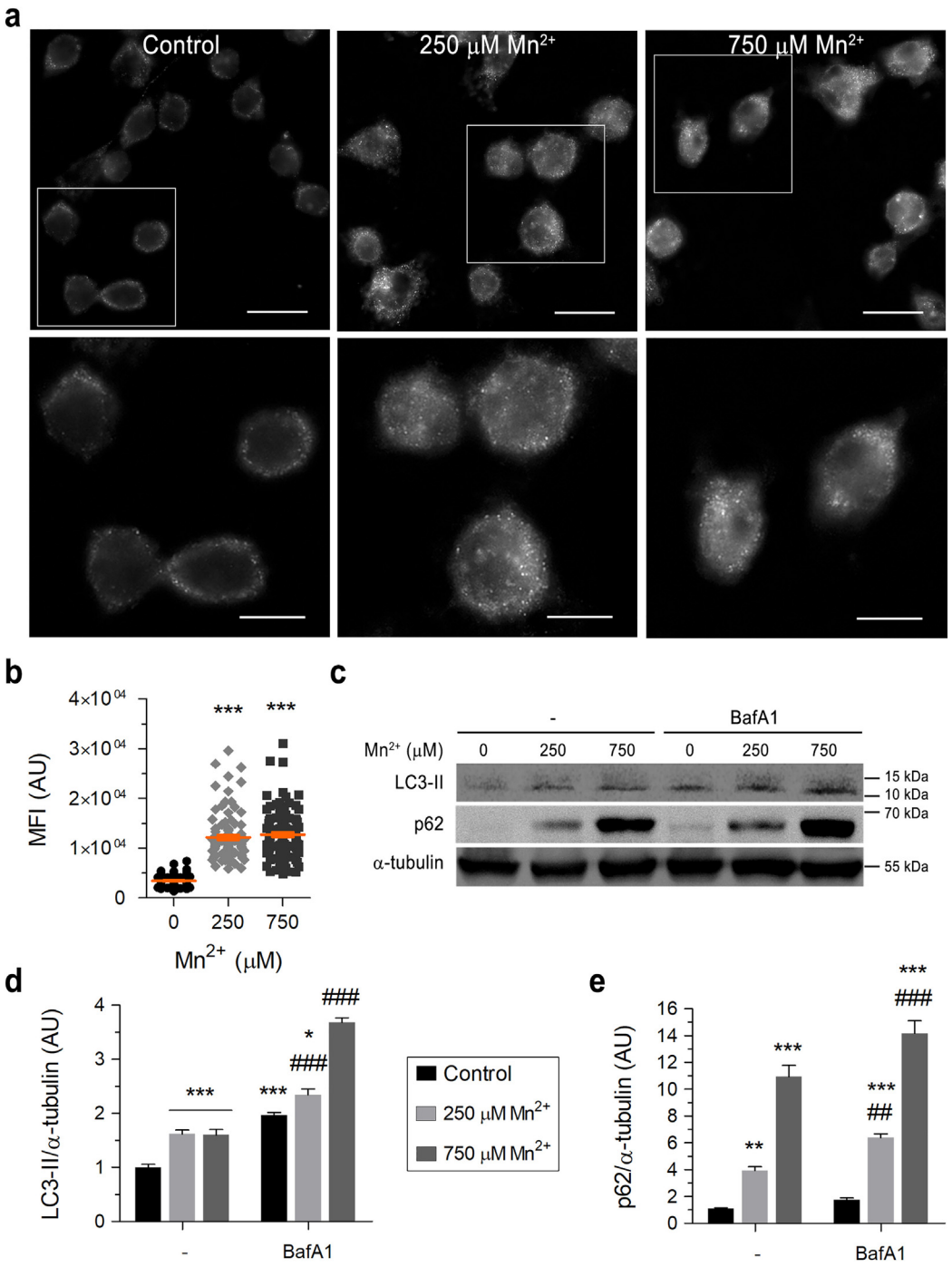

Fig. 3. Mn^{2+} triggers the autophagic flux. (a, b) BV-2 cells were exposed to Mn^{2+} (250 and 750 μM) for 24 h and autophagosomes formation was analyzed by immunofluorescence microscopy. Cells were immunolabeled for LC3 (Alexa 555: λex: 543/20 nm, λem: 593/40 nm). (a) Representative images are shown. Scale bar: 20 μm. Lower panels denote magnification (2.2×) of the selected area; Scale bar: 10 μm. (b) Mean fluorescence intensity of LC3 immunofluorescence was measured employing ImageJ software (100 cells/sample). (c–e) Before the end of Mn^{2+} exposure, BafA1 was added to culture media (100 nM, 2 h) to prevent lysosomal degradation. Total cellular lysates were run on SDS-PAGE. Blots were probed with anti-LC3-II and anti-p62, and normalized to α-tubulin. (c) Representative blots are shown. Relative expression of LC3-II (d) and p62 (e) were analyzed by ImageJ software. Values are expressed as fold of control. *$p < 0.05$, **$p < 0.01$ and ***$p < 0.001$ vs control; ##$p < 0.01$ and ###$p < 0.001$ vs Mn^{2+}.

increment does not unquestionably represent the completion of autophagy. Autophagosomes fuse with lysosomes to form autolysosomes. Blockade of autophagy at this step could also result in an increased number of autophagosomes. In order to distinguish these possibilities we analyzed the autophagic flux by employing BafA1, a widely used inhibitor of autophagosome-lysosome fusion in vitro [46]. Exposure to 250 and 750 μM Mn^{2+} produced an increase in LC3-II expression levels of 61.6 ± 7.5% ($p < 0.01$) and 60.1 ± 9.9% ($p < 0.01$), respectively (Fig. 3c and d), supporting previous results (Fig. 3a and b). In the presence of BafA1, LC3-II levels increased for all conditions assayed: 97.0 ± 5.0% for control cells ($p < 0.001$), 72.9 ± 6.5% for 250 μM Mn^{2+} ($p < 0.001$) and 208.4 ± 5.3% ($p < 0.001$) for 750 μM Mn^{2+}.

Kinetics of p62 levels is also a useful marker of autophagic flux [21]. Our results showed a p62 expression pattern similar to that of LC3-II (Fig. 3c–e). Mn^{2+} induced a 3.9 ± 0.3 and 10.9 ± 0.8-fold increase

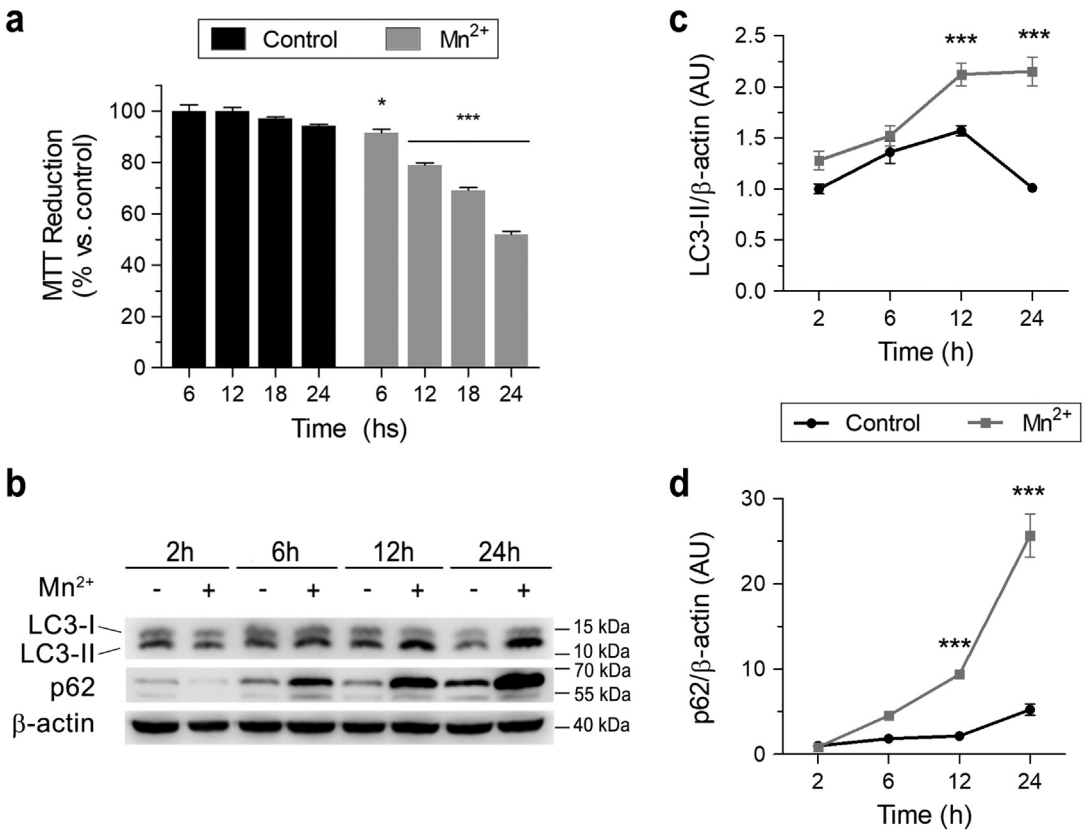

Fig. 4. Autophagy kinetics in Mn^{2+}-exposed microglia. BV-2 cells were exposed to Mn^{2+} (250 μM). (a) Cell viability was measured at different time points (6, 12, 18 and 24 h) by MTT reduction assay. Values are expressed as a percentage of control cells. (b–d) Total cellular lysates of 2, 6, 12 and 24 h Mn^{2+}-exposed cells were run on SDS-PAGE. Blots were probed with anti-LC3-II and anti-p62, and normalized to β-actin. (b) Representative blots are shown. Relative expression of LC3-II (c) and p62 (d) were analyzed by ImageJ software. Values are expressed as fold of control. *$p < 0.05$ and ***$p < 0.001$ vs control.

in p62 expression levels at 250 and 750 μM, respectively. This is in accordance with previous reports describing p62 upregulation accompanied with an increment in the autophagic flux [47]. After BafA1 treatment, we detected a 61.5 ± 11.4 and 29.6 ± 14.4% increase in p62 levels for 250 and 750 μM Mn^{2+} exposed cells, respectively. The increment in both LC3-II and p62 levels in the presence of BafA1 indicates that the autophagy is functional. Altogether our findings demonstrate that Mn^{2+} induces autophagy in BV-2 cells.

3.3. Kinetics and role of autophagy in Mn^{2+}-exposed cells

Autophagy is a complex and dynamic multi-step process. In order to understand the kinetics of the autophagic pathway we conducted experiments by exposing BV-2 cells to 250 μM Mn^{2+} during variable times (2–24 h). The first step was to analyze the cell viability as a function of time (Fig. 4a). Exposure to Mn^{2+} resulted in a time-dependent decrease in cell viability from 91.5 ± 2.5% (6 h Mn^{2+} exposure) ($p < 0.05$) to 52.0 ± 0.7% (24 h Mn^{2+} exposure) ($p < 0.01$). Therefore, we examined autophagy induction by evaluating autophagosomes formation by western blotting (Fig. 4b–c). Both LC3-II and p62 expression levels increased over the time course studied indicating the activation of autophagy.

Afterwards we carried out experiments in order to study the role of autophagy in Mn^{2+} cytotoxicity. For this purpose we assayed the effect of different autophagy modulators: Wort (a class III phosphoinositide-3-kinase, PI3KC3 inhibitor), Rapa (a specific mTORC1 inhibitor and autophagy inducer) and Mel (a recognized autophagy modulator) [48] on LC3-II and p62 expression levels.

As shown in Fig. 5a–c Rapa induced an increase in LC3-II expression levels for 18 h ($p < 0.001$) and 24 h ($p < 0.05$) Mn^{2+} exposure and decrease p62 accumulation for all exposure times assayed (12 h and 18 h: $p < 0.05$; 24 h: $p < 0.001$). Pre-incubation with Mel induced an increment in LC3-II expression levels for 12 h ($p < 0.05$), 18 h ($p < 0.001$) and 24 h ($p < 0.05$). However, unlike what was observed for Rapa, p62 levels increased for 18 h ($p < 0.01$) and 24 h ($p < 0.05$). On the other hand, Wort decreased LC3-II expression levels at all times tested (12 h and 18 h: $p < 0.05$; 24 h: $p < 0.01$) while increasing the levels of p62 only at 18 h ($p < 0.05$). These findings indicate that Rapa and Mel positively modulate autophagy in Mn^{2+} exposed BV-2 cells, whereas Wort inhibits this process.

When cell viability was assessed we observed that both Rapa (7.7 ± 1.8; $p < 0.001$) and Mel (15.5 ± 1.3; $p < 0.001$) induced an increase in cell viability in comparison with those of Mn^{2+} alone for 24 h exposure. Despite the previous results, Wort did not exhibit any effect on cell survival under the assayed conditions.

Finally, to further confirm the roles of Rapa and Mel in positively modulating autophagy, we evaluated the autophagic flux by employing a plasmid encoding a tandem GFP-mCherry-LC3B fusion protein [37]. Considering the dynamic nature of autophagic process (Fig. 4) we performed experiments at two different Mn^{2+} exposition times: 2 h (in the absence of cytotoxicity, Fig. 6) and 24 h (under cell death conditions, Fig. 7).

As shown in Fig. 8a, exposure to Mn^{2+} for 2 h increased significantly the number of autolysosomes per cell (41.8 ± 3.8%; $p < 0.01$ vs control: 24.6 ± 4.9%). A similar effect was observed in BV-2 cells pre-incubated with Rapa both in the presence (46.8 ± 5.3%, not significant vs Mn^{2+}) and absence of Mn^{2+} (49.9 ± 3.8%; $p < 0.01$ vs control). On the other hand, when BafA1 was employed to block the autophagic flux, the number of autolysosomes decreased both in the presence and absence of Mn^{2+} (5.2 ± 2.2%, $p < 0.001$ vs

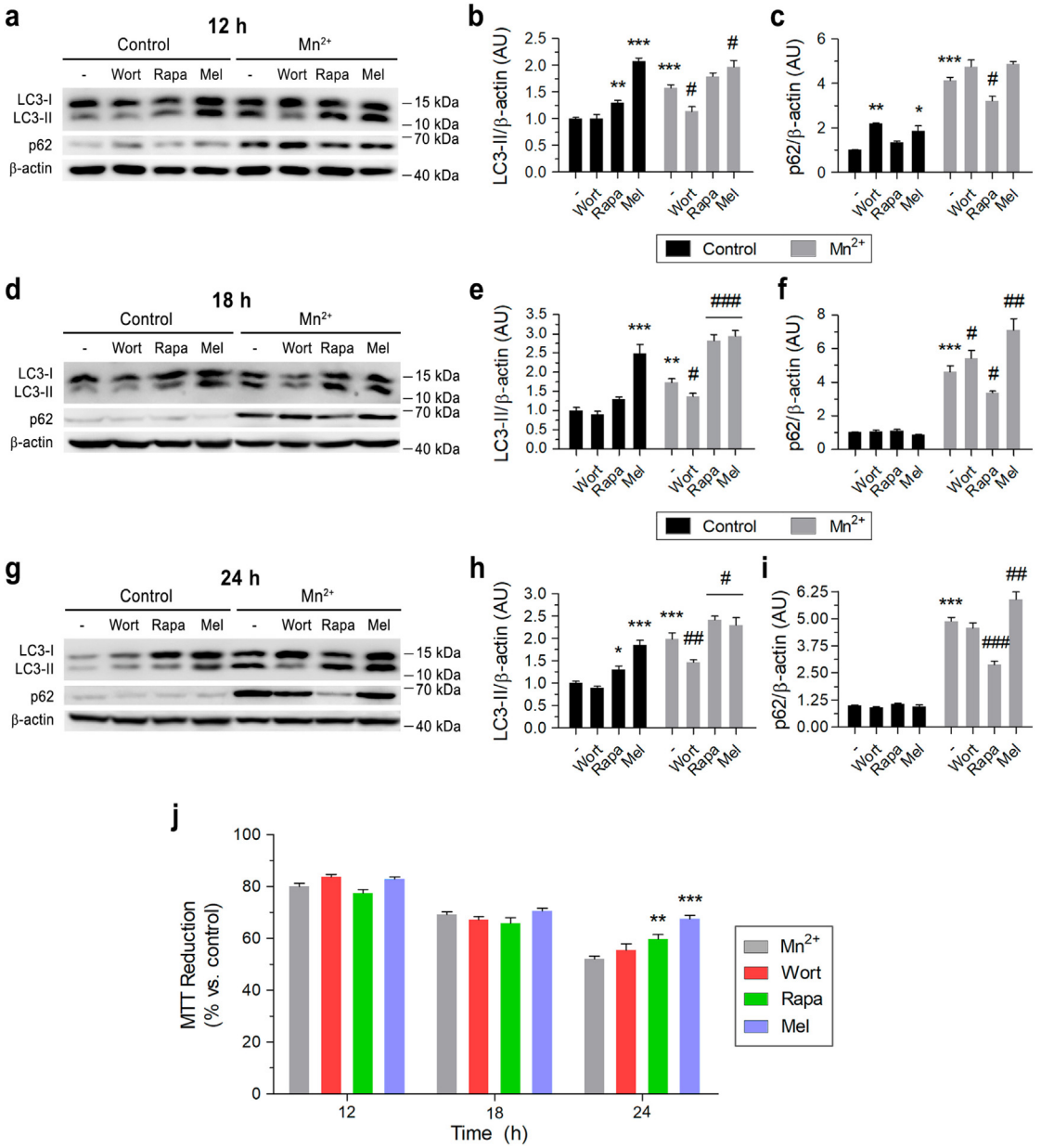

Fig. 5. Modulation of autophagy kinetics in Mn^{2+}-exposed microglia. BV-2 cells were pre-incubated (1 h) with Wort (50 nM), Rapa (200 nM) or Mel (10 μM) and exposed to Mn^{2+} (250 μM). Total cell lysates were collected after 12 h (a–c), 18 h (d–f) and 24 h (g–i), and run on SDS-PAGE. Blots were probed with anti-LC3-II and anti-p62, and normalized to β-actin. (a, d, g) Representative blots are shown. Relative expression of LC3-II (b, e, h) and p62 (c, f, i) were analyzed by ImageJ software. Values are expressed as fold of control. *p < 0.05, **p < 0.01 and ***p < 0.001 vs control; #p < 0.05, ##p < 0.01 and ###p < 0.001 vs Mn^{2+}. (j) Cell viability was measured by MTT reduction assay as a function of time. Values are expressed as a percentage of control cells. **p < 0.01 and ***p < 0.001 vs Mn^{2+}.

control; 18.6 ± 3.7%, p < 0.001 vs Mn^{2+}). Mel did not exhibit relevant effects. At 24 h exposure, Mn^{2+} induced a marked accumulation of autophagosomes (83.6 ± 7.0%; p < 0.05 vs control: 55.9 ± 9.7%) indicating a blockade of autophagic flux (Fig. 8b) which was similar to that observed in control cells incubated with BafA1 (89.4 ± 4.6%, p < 0.05 vs control). In accordance with our previous results (Fig. 5), pre-incubation with both Rapa and Mel increased the amount of autolysosomes in Mn^{2+} exposed cells (57.4 ± 8.2% and 46.9 ± 9.9%, respectively, p < 0.05 vs Mn^{2+}: 16.4 ± 6.9%).

We also analyzed the total amount of vesicles per cell (Fig. 8c and d). At 2 h exposure, only the cells exposed to Mn^{2+} presented an increase in the number of vesicles (35.3 ± 3.5; p < 0.01 vs control: 23.8 ± 2.2). BafA1, Rapa and Mel treatments restored the number of vesicles to the control levels. Interestingly, although the amount of vesicles present at 24 h Mn^{2+} exposure (37.7 ± 4.4) did not show differences respect the control (42.0 ± 5.7), a change in the type of vesicles (autophagosomes and autolysosomes) occurred. On the other hand, pre-incubation with Rapa and Mel increased this parameter (p < 0.05).

In conclusion, our findings indicate that autophagy is activated in Mn^{2+}- treated microglial cells. However, there are differences in the autophagic flux as time passes. At short exposure times, Mn^{2+} do not cause disturbances in the autophagic flux whereas at longer period of exposure, the accumulated damage inside the cell triggers a dysfunction of this mechanism (Fig. 9). Both Rapa and Mel would prevent this disturbance in the autophagic flux increasing the survival of microglial cells.

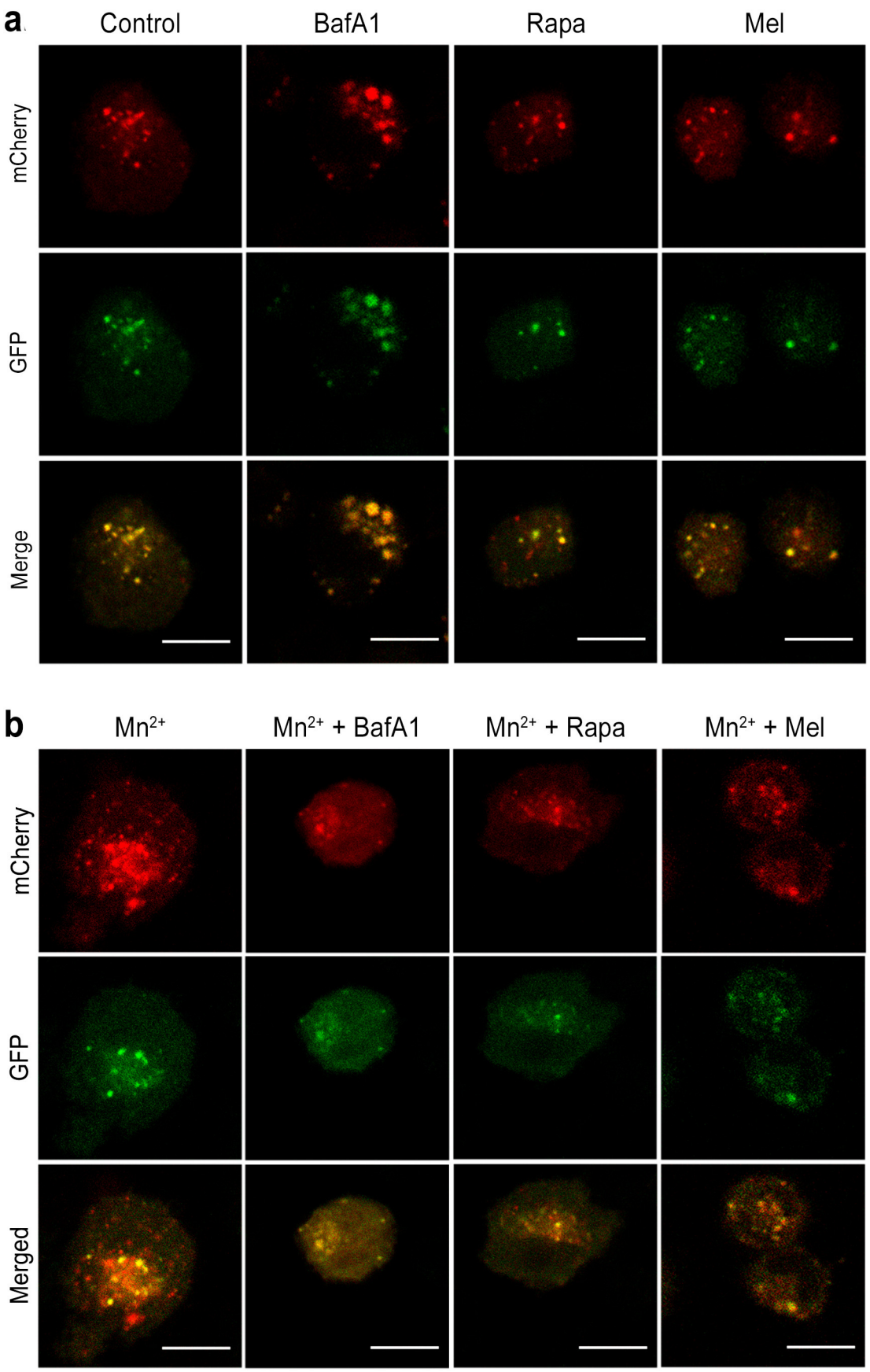

Fig. 6. Autophagic flux at 2 h of Mn^{2+} exposure. BV-2 cells transiently expressing GFP-mCherry-LC3B were pre-incubated (1 h) with Rapa (200 nM) or Mel (10 μM) and exposed to Mn^{2+} (250 μM) for 2 h. To block the autophagic flux, BafA1 was added to culture media (100 nM) at the beginning of the incubation period. Representative confocal images of control (a) and Mn^{2+}-exposed cells (b) are shown. Scale bar: 10 μm.

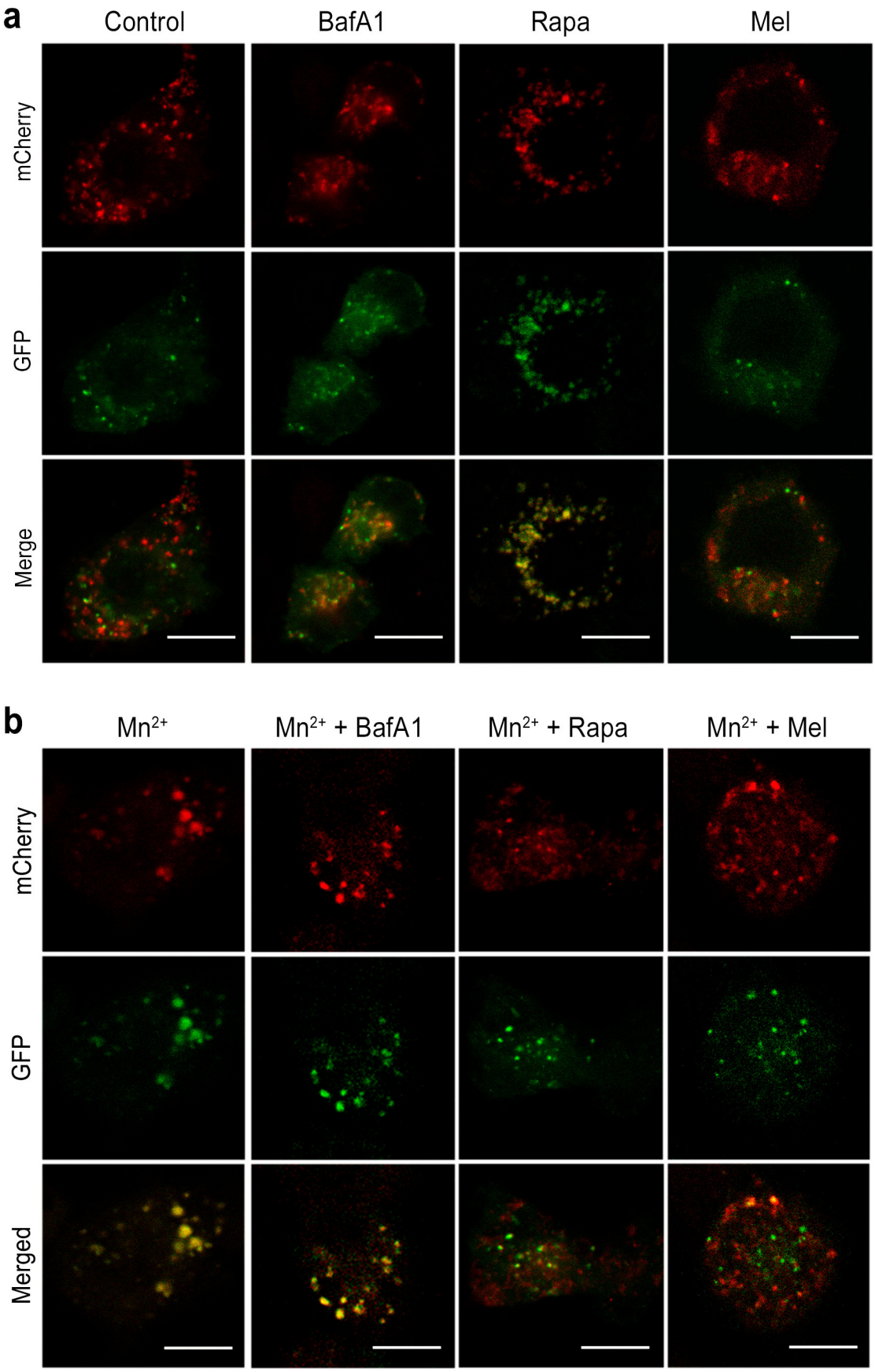

Fig. 7. Autophagic flux at 24 h of Mn^{2+} exposure. BV-2 cells transiently expressing GFP-mCherry-LC3B were pre-incubated (1 h) with Rapa (200 nM) or Mel (10 μM) and exposed to Mn^{2+} (250 μM) for 24 h. BafA1 was added to culture media (100 nM, 2 h) before the end of experiment. Representative confocal images of control (a) and Mn^{2+}-exposed cells (b) are shown. Scale bar: 10 μm.

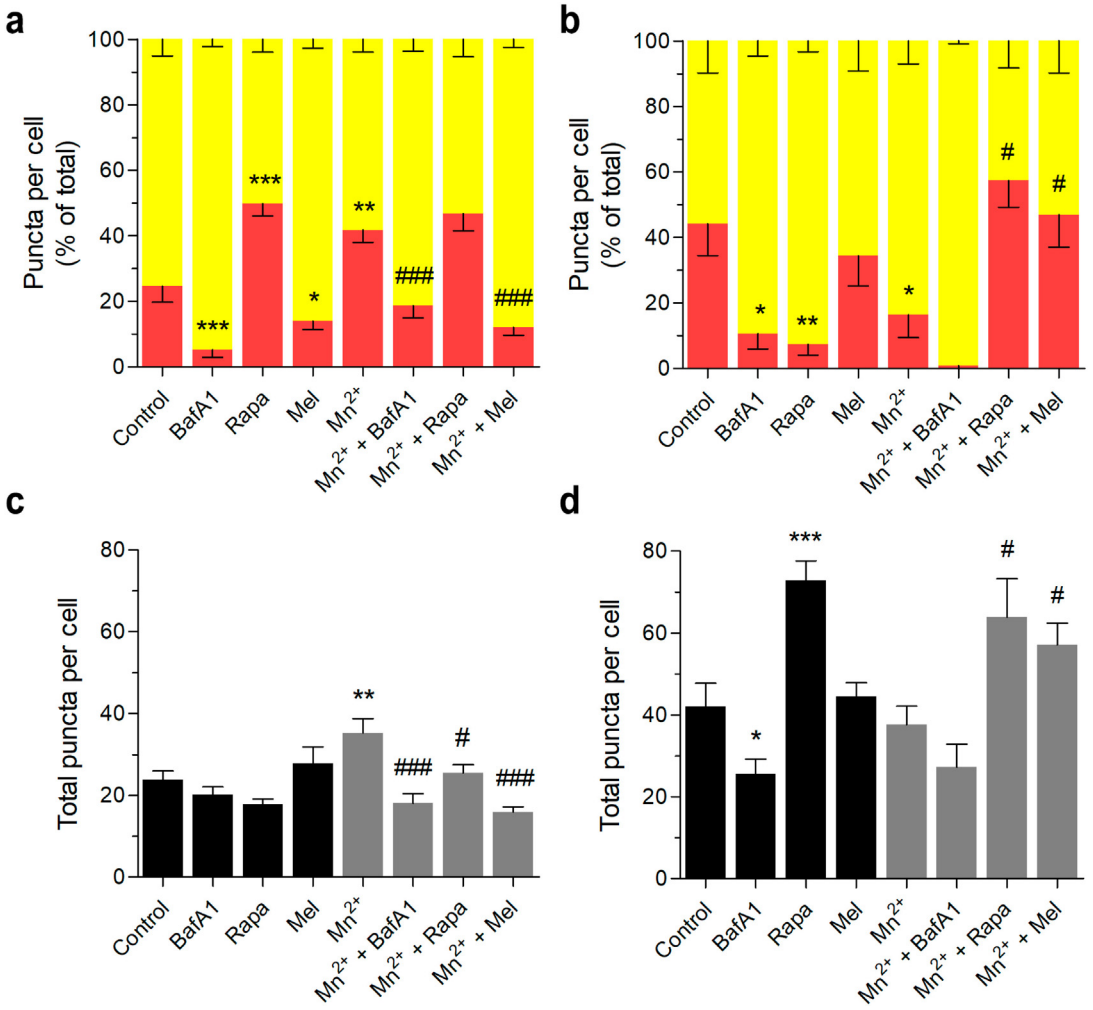

Fig. 8. Modulation of the autophagic flux in Mn^{2+}-exposed cells. GFP-mCherry-LC3B-transfected BV-2 cells were treated with Rapa (200 nM), Mel (10 μM) or BafA1 (100 nM) and exposed to Mn^{2+} (250 μM) for 2 h (a, c) or 24 h (b, d). From images obtained by confocal microscopy, the number of autophagosomes (yellow dots) and autolysosomes (red dots) per cell was quantified (20 cells/sample). (a, b) Values are expressed as percentage of total. (c, d) Graphical quantification of dots per cell. *p < 0.05, **p < 0.01 and ***p < 0.001 vs control; #p < 0.05 and ###p < 0.001 vs Mn^{2+}.

4. Discussion

Evidence accumulated over the past two decades has revealed that Mn-induced neurological injury involves a complex crosstalk between neurons and glial cells mediated by pathophysiological signaling mechanisms. Although main attention was focused on neurons, glial cells are an important target of Mn in the brain. In addition to sequestering Mn, these cells activate inflammatory signaling pathways that damage neurons through overproduction of ROS and RNS and inflammatory cytokines [17]. Particularly, the contribution of microglia to neurodegeneration in manganism has recently become a topic of great interest ([17], and cited references). Nevertheless, the mechanisms involved in this process have been poorly explored.

It has been widely described that Mn enhances ROS production which contributes to its toxicity [49]. Particularly, we have previously demonstrated that Mn^{2+} increases ROS generation in rat primary cortical astrocytes [50], rat C6 glioma cells [51] and microglial BV-2 cells [35]. Furthermore, we revealed that ROS play a critical role in both Mn^{2+}-induced C6 and BV-2 cell death [32,35,51].

The oxidative stress-mediated injury affects cellular organelles mainly mitochondria, lysosomes and endoplasmic reticulum [52,53]. In BV-2 microglial cells we have demonstrated that Mn^{2+} induces LMP and CatD release into the cytosol indicating the occurrence of lysosomal disruption [35]. In the present work we extended that study and provided evidence demonstrating that BV-2 cells exposed to Mn^{2+} exhibit alterations in the AVOs distribution and number (Figs. 1 and 2). Pre-incubation with 10 μM Mel, one of the most effective molecules in neutralizing the oxidant effects of ROS [54], completely prevented the increase in lysosomes number induced by Mn^{2+} without affecting the vesicles diameter. Our present findings show the key role of ROS in our model. These reactive species generated by Mn^{2+} exposure induce lysosomal alterations leading to LMP, cathepsins release and cell death. In addition to the antioxidant actions reported for Mel, another mechanism based in its anti-inflammatory properties could be implied in the protective effect of this hormone on cell viability. In this regard, Park and Chun [55] recently showed that Mel prevents the activation of a pro-inflammatory response in microglia exposed to Mn^{2+}. In our model, where Mn^{2+}-induced BV-2 cell activation was demonstrated [56,57], Mel could act at early stages of activation impairing the inflammatory response.

Autophagy is intimately associated with eukaryotic cell death. However, the molecular connections between both processes are intricate, with autophagy promoting or inhibiting cell death in a context dependent manner [58–60]. Despite the increasing number of studies reporting the effect of autophagy in the CNS homeostasis and disease progression [61], most of the current literature focuses on neurons. Thus, the effects of autophagy and its modulation on microglial cells have been little addressed. We therefore evaluated the possible

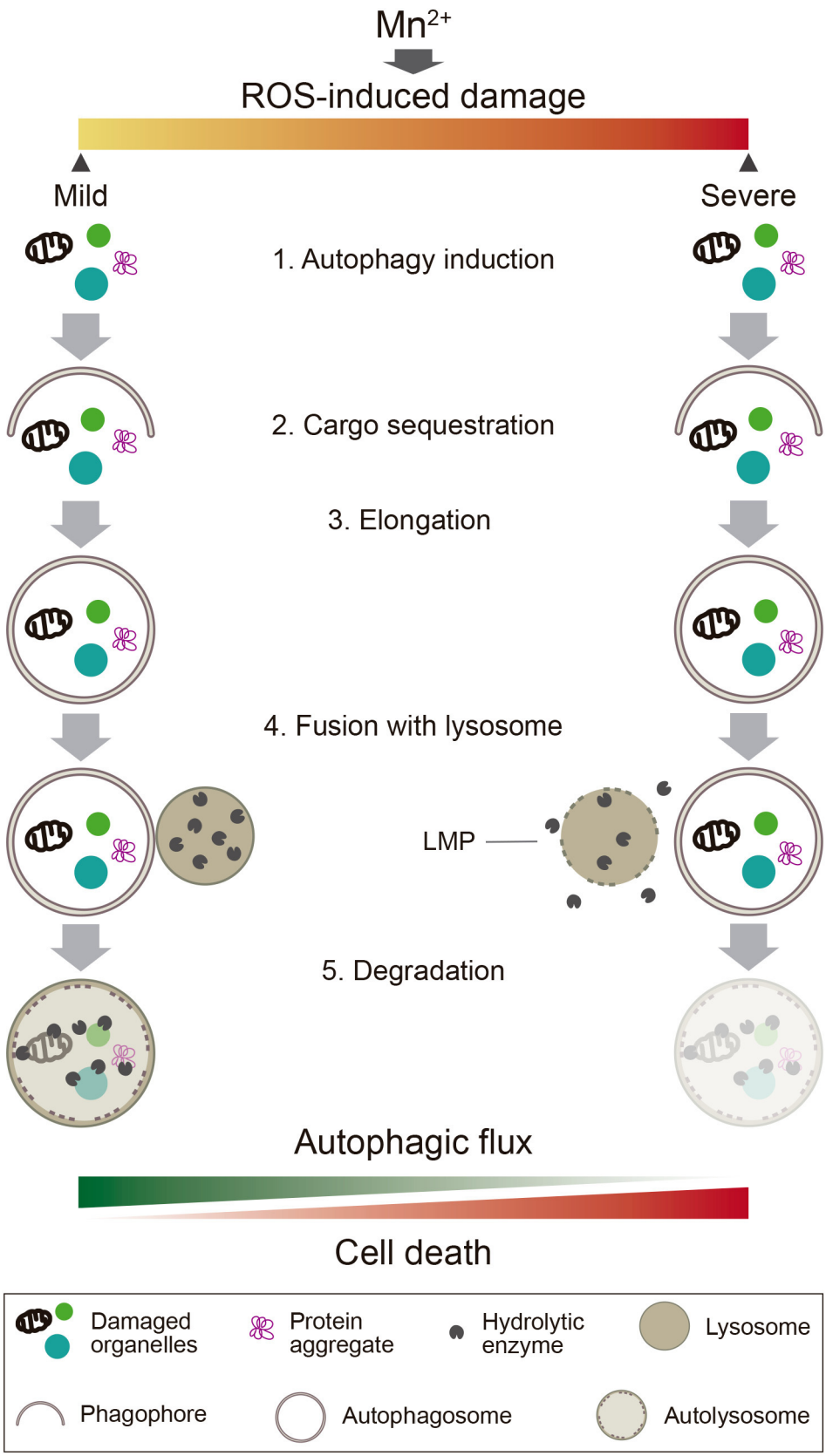

Fig. 9. Proposed model of Mn^{2+}-induced autophagy in BV-2 microglial cells. Mn^{2+}-induced ROS generation results in both organelle and protein damage. These events trigger autophagy as an attempt to restore cellular homeostasis. In conditions of mild damage, autophagy is completed, leading to degradation of injured components and favouring cell survival. When ROS-induced damage accumulates, the formation or degradation of autolysosomes is impaired due to lysosomal membrane permeabilization (LMP). In this scenario, where the autophagic flux is inhibited and cathepsins are release into cytosol, Mn^{2+} triggers microglial cell death.

autophagy activation in Mn^{2+}-exposed BV-2 cells and its role on cell survival. We found that 24 h Mn^{2+} exposure induces autophagy in microglial cells with increased levels of LC3-II and p62 (Fig. 3). As we mentioned above, under these conditions, Mn^{2+} induces LMP accompanied by cathepsins release and increased number of lysosomes. Interestingly, autophagic flux remains, at least in part, functional (Fig. 3c and d). Thus, it is possible that cells trigger autophagy in order to neutralize the risks associated with lysosomal rupture [62].

Considering this role for autophagy, the increase in the number of lysosomes (Fig. 2d) could be considered as an attempt of cells to maintain homeostasis by preserving functional autophagy. These results are in accordance with those of Bussi et al. [63] and Wang et al. [33]. Although autophagy is a highly dynamic pathway, reports regarding this process have been mostly conducted at fixed times. However, an elevated autophagosome content could be due to increased formation or decreased clearance of these vesicles. As a consequence, the measurements of the number of autophagosomes present at a single time point may be misleading in certain circumstances, where lysosomal clearance is impaired [64]. In the present work, we extensively characterized the kinetics of autophagy by performing experiments at different time points after Mn^{2+} stimulation. Results from western blots showed that LC3-II and p62 expression levels are already incremented after 6 h of Mn^{2+} stimulation and progressively increase until 24 h (Fig. 4b–d). In parallel, a decrease in cell viability as a function of time was observed (Fig. 4a). These findings are consistent with our previous results indicating that Mn^{2+} induces BV-2 regulated necrosis in which lysosomal dysfunction plays a critical role [35]. Under this scenario autophagy induction is again shown as a rescue mechanism working towards the elimination of damaged lysosomes.

Finally, in order to define the role of autophagy in our model, we analyzed its modulation at different times after Mn^{2+} stimulation. When Rapa was incubated with Mn^{2+} at different times, increased LC3-II and decreased p62 expression levels were observed in comparison with controls (Fig. 5) (Mn^{2+} alone). The effect on LC3-II was more pronounced at 18 h Mn^{2+} exposure. These data are consistent with Rapa-mediated autophagy activation according to its classical function. The fact that p62 levels show a diminished expression as a function of time seems to controvert the corresponding profile described in Fig. 4. This apparent discrepancy may be explained by a more functional autophagy taking place in the presence of the autophagic activator Rapa. A similar pattern of LC3-II expression levels but peaking at 2 h Rapa exposure was reported by Iwai Kanai et al. [64] in chloroquine-dependent autophagy in cardiac myocytes HL-1. This response can be attributed to different instances of autophagic flux execution involving events such as the lysosomal integrity, the accumulation of autophagosomes, and the disruption of autophagosome-autolysosome fusion. On the other hand, we found that the inhibitory effect of Wort on LC3-II levels remained over time (Fig. 5). Our results are in line with those of Wu et al. [65], who reported a persistent inhibition of PI3KC3 by Wort (50 nM). Incubation with Mel in the presence of Mn^{2+} resulted in increased expression levels of both LC3-II and p62 at 18 h and 24 h exposure. Although the result obtained for p62 was unexpected, the fact that p62 status is sometimes cell type and context specific could explain it [47].

Autophagy activation described for both Rapa and Mel was confirmed by employing the plasmid encoding a tandem GFP-mCherry-LC3B fusion protein [37] (Figs. 6–8). This autophagy activation resulted in increased cell viability for 24 h Mn^{2+} exposed cells (Fig. 5d). These findings demonstrate that autophagy plays a protective role in Mn^{2+}-induced cell death in microglial cells. Similar results were obtained by our group employing C6 cells exposed to Mn^{2+} [32].Thus, the effect of these modulators on cell viability was observed later (24 h) to those corresponding to the higher expression levels of LC3-II and p62 (18 h) (Fig. 5a–c).

Mel has been classically related to the physiological regulation of seasonal and circadian rhythms [66]. In addition, its antioxidant properties were widely described in different experimental models [67,68]. More recently it has been reported that Mel may modulate the autophagic process in different in vitro and in vivo models [48]. Particularly, Mel-induced autophagy protected SH-SY5Y cells from prion protein-induced neurotoxicity [69]. Similarly, Mel reduced cadmium-induced neurotoxicity by regulating both the autophagic-related pathways and proteins [70]. These findings strongly support the fact that Mel induces its beneficial effects through autophagy promotion. In our model we have demonstrated that Mel increases the autophagic flux which remains functional even in the presence of Mn^{2+} (Figs. 5–8). Taking into account that Mel is a promise molecule in the treatment of several neurodegenerative diseases [71–73] regulation of autophagy by Mel is a determinant parameter that should be considered in the future studies focused in manganism, parkinsonisms and possibly other neurodegenerative therapeutic strategies.

In summary, this manuscript provides new insights about the effects of Mn on lysosomal integrity in BV-2 cells. Moreover, we described in detail, for the first time, the dynamic and modulation of microglial autophagy and their impact on cell survival. We propose that autophagy is triggered as a rescue mechanism in an attempt to protect cells from lethal effects of Mn. Future research will shed light on the cellular targets and molecular pathways involved in the protective effect of autophagy in our experimental model.

CRediT authorship contribution statement

Soledad Porte Alcon: Conceptualization, Data curation, Formal analysis, Investigation, Methodology, Writing - original draft, Writing - review & editing. **Roxana Mayra Gorojod:** Formal analysis, Investigation, Methodology, Resources, Writing - review & editing. **Mónica Lidia Kotler:** Conceptualization, Formal analysis, Funding acquisition, Investigation, Project administration, Resources, Writing - original draft, Writing - review & editing.

Declaration of competing interest

The authors declare that they have no known competing financial interests or personal relationships that could have appeared to influence the work reported in this paper.

Acknowledgements

This work was supported by grants from the Consejo Nacional de Investigaciones Científicas y Técnicas (CONICET, Grants PIP 0771 and 0519) and Agencia Nacional de Promoción Científica y Tecnológica (ANPCYT, PICT 2017-3296). The authors thank Dr. Flavia Saravia (QB-FCEN-UBA, IBYME-CONICET) for providing relevant materials and Dr. Sergio Nemirovsky for his valuable contribution to statistical analysis. S.P.A. is supported by a CONICET Postdoctoral scholarship. R.M.G. is Head Teaching Assistant at Department of Biological Chemistry (FCEN-UBA). M.L.K. is a Principal Researcher at CONICET.

References

[1] V. Schramm, Manganese in Metabolism and Enzyme Function, 1st ed., Academic Press, 1986. https://www.elsevier.com/books/manganese-in-metabolism-and-enzyme-function/schramm/978-0-12-629050-9 (accessed July 16, 2017).
[2] A. Takeda, Manganese action in brain function, Brain Res. Brain Res. Rev. 41 (2003) 79–87.
[3] M. Aschner, K. Erikson, Manganese, Adv. Nutr. Bethesda Md. 8 (2017) 520–521, https://doi.org/10.3945/an.117.015305.
[4] M. Williams, G.D. Todd, N. Roney, J. Crawford, C. Coles, P.R. McClure, J.D. Garey, K. Zaccaria, M. Citra, Toxicological Profile for Manganese, Agency for Toxic Substances and Disease Registry (US), Atlanta (GA), http://www.ncbi.nlm.nih.gov/books/NBK158872/, (2012).
[5] J.H. Freeland-Graves, T.Y. Mousa, S. Kim, International variability in diet and requirements of manganese: causes and consequences, J. Trace Elem. Med. Biol. Organ Soc. Miner. Trace Elem. GMS. 38 (2016) 24–32, https://doi.org/10.1016/j.jtemb.2016.05.004.
[6] C.G. Fraga, Relevance, essentiality and toxicity of trace elements in human health, Mol. Asp. Med. 26 (2005) 235–244, https://doi.org/10.1016/j.mam.2005.07.013.
[7] M. Aschner, T.R. Guilarte, J.S. Schneider, W. Zheng, Manganese: recent advances in understanding its transport and neurotoxicity, Toxicol. Appl. Pharmacol. 221 (2007) 131–147, https://doi.org/10.1016/j.taap.2007.03.001.
[8] J.A. Roth, Are there common biochemical and molecular mechanisms controlling manganism and parkisonism, NeuroMolecular Med. 11 (2009) 281–296, https://doi.org/10.1007/s12017-009-8088-8.
[9] A.B. Bowman, G.F. Kwakye, E. Herrero Hernández, M. Aschner, Role of manganese in neurodegenerative diseases, J. Trace Elem. Med. Biol. Organ Soc. Miner. Trace

Elem. GMS. 25 (2011) 191–203, https://doi.org/10.1016/j.jtemb.2011.08.144.
[10] J. Couper, On the effects of black oxide of manganese when inhaled in the lungs, Br Ann Med Pharmacol. 1 (1837) 41–42.
[11] K. Tuschl, P.B. Mills, P.T. Clayton, Chapter twelve - manganese and the brain, in: K.P. Bhatia, S.A. Schneider (Eds.), Int. Rev. Neurobiol, Academic Press, 2013, pp. 277–312, , https://doi.org/10.1016/B978-0-12-410502-7.00013-2.
[12] S.L. O'Neal, W. Zheng, Manganese toxicity upon overexposure: a decade in review, Curr. Environ. Health Rep. 2 (2015) 315–328, https://doi.org/10.1007/s40572-015-0056-x.
[13] T.V. Peres, M.R.C. Schettinger, P. Chen, F. Carvalho, D.S. Avila, A.B. Bowman, M. Aschner, "Manganese-induced neurotoxicity: a review of its behavioral consequences and neuroprotective strategies," BMC Pharmacol. Toxicol. 17 (2016). doi:https://doi.org/10.1186/s40360-016-0099-0.
[14] Y.S. Kim, T.H. Joh, Microglia, major player in the brain inflammation: their roles in the pathogenesis of Parkinson's disease, Exp. Mol. Med. 38 (2006) 333–347, https://doi.org/10.1038/emm.2006.40.
[15] M.E. Lull, M.L. Block, Microglial activation and chronic neurodegeneration, Neurother. J. Am. Soc. Exp. Neurother. 7 (2010) 354–365, https://doi.org/10.1016/j.nurt.2010.05.014.
[16] W.J. Streit, R.E. Mrak, W.S.T. Griffin, Microglia and neuroinflammation: a pathological perspective, J. Neuroinflammation 1 (2004) 14, https://doi.org/10.1186/1742-2094-1-14.
[17] R.B. Tjalkens, K.A. Popichak, K.A. Kirkley, Inflammatory activation of microglia and astrocytes in manganese neurotoxicity, Adv. Neurobiol. 18 (2017) 159–181, https://doi.org/10.1007/978-3-319-60189-2_8.
[18] N.M. Filipov, C.A. Dodd, Role of glial cells in manganese neurotoxicity, J. Appl. Toxicol. JAT. 32 (2012) 310–317, https://doi.org/10.1002/jat.1762.
[19] B. Halliwell, M. Whiteman, Measuring reactive species and oxidative damage in vivo and in cell culture: how should you do it and what do the results mean? Br. J. Pharmacol. 142 (2004) 231–255, https://doi.org/10.1038/sj.bjp.0705776.
[20] N. Mizushima, T. Yoshimori, B. Levine, Methods in mammalian autophagy research, Cell 140 (2010) 313–326, https://doi.org/10.1016/j.cell.2010.01.028.
[21] S. Pankiv, T.H. Clausen, T. Lamark, A. Brech, J.-A. Bruun, H. Outzen, A. Øvervatn, G. Bjørkøy, T. Johansen, p62/SQSTM1 binds directly to Atg8/LC3 to facilitate degradation of ubiquitinated protein aggregates by autophagy, J. Biol. Chem. 282 (2007) 24131–24145, https://doi.org/10.1074/jbc.M702824200.
[22] G. Kroemer, G. Mariño, B. Levine, Autophagy and the integrated stress response, Mol. Cell 40 (2010) 280–293, https://doi.org/10.1016/j.molcel.2010.09.023.
[23] D.J. Klionsky, P. Codogno, The mechanism and physiological function of macroautophagy, J. Innate Immun. 5 (2013) 427–433, https://doi.org/10.1159/000351979.
[24] G. Filomeni, D. De Zio, F. Cecconi, Oxidative stress and autophagy: the clash between damage and metabolic needs, Cell Death Differ. 22 (2015) 377–388, https://doi.org/10.1038/cdd.2014.150.
[25] A. Eisenberg-Lerner, S. Bialik, H.-U. Simon, A. Kimchi, Life and death partners: apoptosis, autophagy and the cross-talk between them, Cell Death Differ. 16 (2009) 966–975, https://doi.org/10.1038/cdd.2009.33.
[26] Z. Zhang, M. Miah, M. Culbreth, M. Aschner, Autophagy in neurodegenerative diseases and metal neurotoxicity, Neurochem. Res. 41 (2016) 409–422, https://doi.org/10.1007/s11064-016-1844-x.
[27] J. Zhang, R. Cao, T. Cai, M. Aschner, F. Zhao, T. Yao, Y. Chen, Z. Cao, W. Luo, J. Chen, The role of autophagy dysregulation in manganese-induced dopaminergic neurodegeneration, Neurotox. Res. 24 (2013) 478–490, https://doi.org/10.1007/s12640-013-9392-5.
[28] Y.K. Tai, K.C.M. Chew, B.W.Q. Tan, K.-L. Lim, T.W. Soong, Iron mitigates DMT1-mediated manganese cytotoxicity via the ASK1-JNK signaling axis: implications of iron supplementation for manganese toxicity, Sci. Rep. 6 (2016) 21113, https://doi.org/10.1038/srep21113.
[29] C. Liu, D.-Y. Yan, X. Tan, Z. Ma, C. Wang, Y. Deng, W. Liu, T.-Y. Yang, Z.-F. Xu, B. Xu, Effect of the cross-talk between autophagy and endoplasmic reticulum stress on Mn-induced alpha-synuclein oligomerization, Environ. Toxicol. 33 (2018) 315–324, https://doi.org/10.1002/tox.22518.
[30] Q. Zhou, X. Fu, X. Wang, Q. Wu, Y. Lu, J. Shi, J.E. Klaunig, S. Zhou, Autophagy plays a protective role in Mn-induced toxicity in PC12 cells, Toxicology 394 (2018) 45–53, https://doi.org/10.1016/j.tox.2017.12.001.
[31] B. Vijayan, V. Raj, S. Nandakumar, A. Kishore, A. Thekkuveettil, Spermine protects alpha-synuclein expressing dopaminergic neurons from manganese-induced degeneration, Cell Biol. Toxicol. 35 (2019) 147–159, https://doi.org/10.1007/s10565-018-09449-1.
[32] R.M. Gorojod, A. Alaimo, S. Porte Alcon, C. Pomilio, F. Saravia, M.L. Kotler, The autophagic- lysosomal pathway determines the fate of glial cells under manganese-induced oxidative stress conditions, Free Radic. Biol. Med. 87 (2015) 237–251, https://doi.org/10.1016/j.freeradbiomed.2015.06.034.
[33] D. Wang, J. Zhang, W. Jiang, Z. Cao, F. Zhao, T. Cai, M. Aschner, W. Luo, The role of NLRP3-CASP1 in inflammasome-mediated neuroinflammation and autophagy dysfunction in manganese-induced, hippocampal-dependent impairment of learning and memory ability, Autophagy 13 (2017) 914–927, https://doi.org/10.1080/15548627.2017.1293766.
[34] J. Chen, P. Su, W. Luo, J. Chen, Role of LRRK2 in manganese-induced neuroinflammation and microglial autophagy, Biochem. Biophys. Res. Commun. 498 (2018) 171–177, https://doi.org/10.1016/j.bbrc.2018.02.007.
[35] S. Porte Alcon, R.M. Gorojod, M.L. Kotler, Regulated necrosis orchestrates microglial cell death in manganese-induced toxicity, Neuroscience 393 (2018) 206–225, https://doi.org/10.1016/j.neuroscience.2018.10.006.
[36] E. Blasi, R. Barluzzi, V. Bocchini, R. Mazzolla, F. Bistoni, Immortalization of murine microglial cells by a v-raf/v-myc carrying retrovirus, J. Neuroimmunol. 27 (1990) 229–237.
[37] C. Pomilio, R.M. Gorojod, M. Riudavets, A. Vinuesa, J. Presa, A. Gregosa, M. Bentivegna, A. Alaimo, S.P. Alcon, G. Sevlever, M.L. Kotler, J. Beauquis, F. Saravia, Microglial autophagy is impaired by prolonged exposure to β-amyloid peptides: evidence from experimental models and Alzheimer's disease patients, GeroScience, (2020), https://doi.org/10.1007/s11357-020-00161-9.
[38] G. Repetto, A. del Peso, J.L. Zurita, Neutral red uptake assay for the estimation of cell viability/cytotoxicity, Nat. Protoc. 3 (2008) 1125–1131, https://doi.org/10.1038/nprot.2008.75.
[39] G. Ates, T. Vanhaecke, V. Rogiers, R.M. Rodrigues, Assaying cellular viability using the neutral red uptake assay., Methods Mol. Biol. Clifton NJ. 1601 (2017) 19–26. doi:https://doi.org/10.1007/978-1-4939-6960-9_2.
[40] A. Alaimo, R.M. Gorojod, J. Beauquis, M.J. Muñoz, F. Saravia, M.L. Kotler, Deregulation of mitochondria-shaping proteins Opa-1 and Drp-1 in manganese-induced apoptosis, PLoS One 9 (2014) e91848, , https://doi.org/10.1371/journal.pone.0091848.
[41] T. Mosmann, Rapid colorimetric assay for cellular growth and survival: application to proliferation and cytotoxicity assays, J. Immunol. Methods 65 (1983) 55–63.
[42] R. Jia, C.M. Guardia, J. Pu, Y. Chen, J.S. Bonifacino, BORC coordinates encounter and fusion of lysosomes with autophagosomes, Autophagy 13 (2017) 1648–1663, https://doi.org/10.1080/15548627.2017.1343768.
[43] E.-L. Eskelinen, P. Saftig, Autophagy: a lysosomal degradation pathway with a central role in health and disease, Biochim. Biophys. Acta 1793 (2009) 664–673, https://doi.org/10.1016/j.bbamcr.2008.07.014.
[44] L. Galluzzi, I. Vitale, J.M. Abrams, E.S. Alnemri, E.H. Baehrecke, M.V. Blagosklonny, T.M. Dawson, V.L. Dawson, W.S. El-Deiry, S. Fulda, E. Gottlieb, D.R. Green, M.O. Hengartner, O. Kepp, R.A. Knight, S. Kumar, S.A. Lipton, X. Lu, F. Madeo, W. Malorni, P. Mehlen, G. Nuñez, M.E. Peter, M. Piacentini, D.C. Rubinsztein, Y. Shi, H.-U. Simon, P. Vandenabeele, E. White, J. Yuan, B. Zhivotovsky, G. Melino, G. Kroemer, Molecular definitions of cell death subroutines: recommendations of the Nomenclature Committee on Cell Death 2012, Cell Death Differ. 19 (2012) 107–120, https://doi.org/10.1038/cdd.2011.96.
[45] V.N. Pivtoraiko, S.L. Stone, K.A. Roth, J.J. Shacka, Oxidative stress and autophagy in the regulation of lysosome-dependent neuron death, Antioxid. Redox Signal. 11 (2009) 481–496, https://doi.org/10.1089/ars.2008.2263.
[46] C. Mauvezin, T.P. Neufeld, Bafilomycin A1 disrupts autophagic flux by inhibiting both V-ATPase-dependent acidification and Ca-P60A/SERCA-dependent autophagosome-lysosome fusion, Autophagy 11 (2015) 1437–1438, https://doi.org/10.1080/15548627.2015.1066957.
[47] D.J. Klionsky, K. Abdelmohsen, A. Abe, M.J. Abedin, H. Abeliovich, A. Acevedo Arozena, H. Adachi, C.M. Adams, P.D. Adams, K. Adeli, P.J. Adhihetty, S.G. Adler, G. Agam, R. Agarwal, M.K. Aghi, et al., Guidelines for the use and interpretation of assays for monitoring autophagy (3rd edition), Autophagy 12 (2016) 1–222, https://doi.org/10.1080/15548627.2015.1100356.
[48] A. Roohbakhsh, A. Shamsizadeh, A.W. Hayes, R.J. Reiter, G. Karimi, Melatonin as an endogenous regulator of diseases: the role of autophagy, Pharmacol. Res. 133 (2018) 265–276, https://doi.org/10.1016/j.phrs.2018.01.022.
[49] E.J. Martinez-Finley, C.E. Gavin, M. Aschner, T.E. Gunter, Manganese neurotoxicity and the role of reactive oxygen species, Free Radic. Biol. Med. 62 (2013) 65–75, https://doi.org/10.1016/j.freeradbiomed.2013.01.032.
[50] L.E. Gonzalez, A.A. Juknat, A.J. Venosa, N. Verrengia, M.L. Kotler, Manganese activates the mitochondrial apoptotic pathway in rat astrocytes by modulating the expression of proteins of the Bcl-2 family, Neurochem. Int. 53 (2008) 408–415, https://doi.org/10.1016/j.neuint.2008.09.008.
[51] A. Alaimo, R. Gorojod, M. Kotler, The extrinsic and intrinsic apoptotic pathways are involved in manganese toxicity in rat astrocytoma C6 cells, Neurochem. Int. 59 (2011) 297–308, https://doi.org/10.1016/j.neuint.2011.06.001.
[52] R.M. Gorojod, A. Alaimo, S. Porte Alcon, F. Saravia, M.L. Kotler, Interplay between lysosomal, mitochondrial and death receptor pathways during manganese-induced apoptosis in glial cells, Arch. Toxicol. (2017), https://doi.org/10.1007/s00204-017-1936-7.
[53] M. Smith, S. Wilkinson, ER homeostasis and autophagy, Essays Biochem. 61 (2017) 625–635, https://doi.org/10.1042/EBC20170092.
[54] R. Reiter, J. Mayo, D. Tan, R. Sainz, M. Alatorre-Jimenez, L. Qin, Melatonin as an antioxidant: under promises but over delivers, J. Pineal Res. 61 (2016) 253–278, https://doi.org/10.1111/jpi.12360.
[55] E. Park, H.S. Chun, Melatonin attenuates manganese and lipopolysaccharide-induced inflammatory activation of BV2 microglia, Neurochem. Res. 42 (2017) 656–666, https://doi.org/10.1007/s11064-016-2122-7.
[56] S. Porte Alcon, E.A. Miglietta, R.M. Gorojod, A. Alaimo, M.L. Kotler, El manganeso induce muerte celular y activación de las células microgliales murinas BV2, Medicina (Mex.). 74 (2014) 175.
[57] S. Porte Alcon, A. Alaimo, R.M. Gorojod, M.L. Kotler, Vías de muerte celular inducida por Mn en células microgliales BV2, Medicina (Mex.). 75 (2015) 93.
[58] K. Degenhardt, R. Mathew, B. Beaudoin, K. Bray, D. Anderson, G. Chen, C. Mukherjee, Y. Shi, C. Gélinas, Y. Fan, D.A. Nelson, S. Jin, E. White, Autophagy promotes tumor cell survival and restricts necrosis, inflammation, and tumorigenesis, Cancer Cell 10 (2006) 51–64, https://doi.org/10.1016/j.ccr.2006.06.001.
[59] D.S. Arroyo, J.A. Soria, E.A. Gaviglio, C. Garcia-Keller, L.M. Cancela, M.C. Rodriguez-Galan, J.M. Wang, P. Iribarren, Toll-like receptor 2 ligands promote microglial cell death by inducing autophagy, FASEB J. 27 (2013) 299–312, https://doi.org/10.1096/fj.12-214312.
[60] D.R. Green, B. Levine, To be or not to be? How selective autophagy and cell death govern cell fate, Cell 157 (2014) 65–75, https://doi.org/10.1016/j.cell.2014.02.049.
[61] R.A. Frake, T. Ricketts, F.M. Menzies, D.C. Rubinsztein, Autophagy and

neurodegeneration, J. Clin. Invest. 125 (2015) 65–74, https://doi.org/10.1172/JCI73944.
[62] I. Maejima, A. Takahashi, H. Omori, T. Kimura, Y. Takabatake, T. Saitoh, A. Yamamoto, M. Hamasaki, T. Noda, Y. Isaka, T. Yoshimori, Autophagy sequesters damaged lysosomes to control lysosomal biogenesis and kidney injury, EMBO J. 32 (2013) 2336–2347, https://doi.org/10.1038/emboj.2013.171.
[63] C. Bussi, J.M.P. Ramos, D.S. Arroyo, E.A. Gaviglio, J.I. Gallea, J.M. Wang, M.S. Celej, P. Iribarren, Autophagy down regulates pro-inflammatory mediators in BV2 microglial cells and rescues both LPS and alpha-synuclein induced neuronal cell death, Sci. Rep. 7 (2017) 43153, https://doi.org/10.1038/srep43153.
[64] E. Iwai-Kanai, H. Yuan, C. Huang, M.R. Sayen, C.N. Perry-Garza, L. Kim, R.A. Gottlieb, A method to measure cardiac autophagic flux in vivo, Autophagy 4 (2008) 322–329, https://doi.org/10.4161/auto.5603.
[65] Y.-T. Wu, H.-L. Tan, G. Shui, C. Bauvy, Q. Huang, M.R. Wenk, C.-N. Ong, P. Codogno, H.-M. Shen, Dual role of 3-methyladenine in modulation of autophagy via different temporal patterns of inhibition on class I and III phosphoinositide 3-kinase, J. Biol. Chem. 285 (2010) 10850–10861, https://doi.org/10.1074/jbc.M109.080796.
[66] J. Arendt, Melatonin and the pineal gland: influence on mammalian seasonal and circadian physiology, Rev. Reprod. 3 (1998) 13–22.
[67] D. Tan, R.J. Reiter, L.C. Manchester, M. Yan, M. El-Sawi, R.M. Sainz, J.C. Mayo, R. Kohen, M. Allegra, R. Hardeland, Chemical and physical properties and potential mechanisms: melatonin as a broad spectrum antioxidant and free radical scavenger, Curr. Top. Med. Chem. 2 (2002) 181–197.
[68] Z. Jiki, S. Lecour, F. Nduhirabandi, Cardiovascular benefits of dietary melatonin: a myth or a reality?, Front. Physiol. 9 (2018). doi:https://doi.org/10.3389/fphys.2018.00528.
[69] J.-K. Jeong, M.-H. Moon, Y.-J. Lee, J.-W. Seol, S.-Y. Park, Melatonin-induced autophagy protects against human prion protein-mediated neurotoxicity, J. Pineal Res. 53 (2012) 138–146, https://doi.org/10.1111/j.1600-079X.2012.00980.x.
[70] M. Li, H. Pi, Z. Yang, R.J. Reiter, S. Xu, X. Chen, C. Chen, L. Zhang, M. Yang, Y. Li, P. Guo, G. Li, M. Tu, L. Tian, J. Xie, M. He, Y. Lu, M. Zhong, Y. Zhang, Z. Yu, Z. Zhou, Melatonin antagonizes cadmium-induced neurotoxicity by activating the transcription factor EB-dependent autophagy-lysosome machinery in mouse neuroblastoma cells, J. Pineal Res. 61 (2016) 353–369, https://doi.org/10.1111/jpi.12353.
[71] P. Wongprayoon, P. Govitrapong, Melatonin as a mitochondrial protector in neurodegenerative diseases, Cell. Mol. Life Sci. CMLS. 74 (2017) 3999–4014, https://doi.org/10.1007/s00018-017-2614-x.
[72] D.P. Cardinali, Melatonin: clinical perspectives in neurodegeneration, Front. Endocrinol. 10 (2019) 480, https://doi.org/10.3389/fendo.2019.00480.
[73] M. Shukla, V. Chinchalongporn, P. Govitrapong, R.J. Reiter, The role of melatonin in targeting cell signaling pathways in neurodegeneration, Ann. N. Y. Acad. Sci. 1443 (2019) 75–96, https://doi.org/10.1111/nyas.14005.